Draft version September 1, 2021
Typeset using LaTeX default style in AASTeX631

Pressure Profiles from Improved Noise Quantification

Daniel R. Hancock[1, 2, 3] and Charles Romero[3, 4]

[1] National Radio Astronomy Observatory
[2] Bridgewater College
[3] Green Bank Observatory
[4] University of Pennsylvania

ABSTRACT

We present pressure profiles of galaxy clusters determined by high resolution Sunyeav-Zel'dovich (SZ) observations from the MUSTANG-2 Bolometer on the Green Bank Telescope. The clusters span a redshift of (0.291-1.14) and are modelled as one or more spheres representing the independent subclusters. We introduce a change in technique from previous papers where we no longer assume the noise to be independent. To account for this change, we look at the covariance matrix of a noise map for each cluster and implement that into our model. Additionally, we constructed non-parametric (NP) fits of our independent noise model, as well as the A10 model for both M_{500} values from both the literature and our model. We have also provided a qualitative analysis of comparisons between the two models discussed in this paper and data from the Archive of Chandra Cluster Entropy Profile Tables (ACCEPT), pending a more in depth analysis of our results. Our covariance model showcases variations in agreement between the independent noise model, the A10 model, and ACCEPT data in all four clusters, but in general, kept a similar shape to the A10 model aside from the occasional outlier, frequently found on the endpoints. The independent noise model has very similar comparisons to the A10 model as the covariance model. Comparing the independent noise model and the covariance model results in a consistent shape, with the exception of occasional deviations, primarily in the endpoints. Furthermore, the covariance model specifically, when looking at the residual, produced overfits and underfits for the bulk pressure parameters, while the independent noise model appeared to provide more consistent residuals.

Keywords: Sunyaev-Zel'dovich Effect — Noise Quantification — Electron pressure

1. INTRODUCTION

Galaxy clusters are among the most massive objects in the universe. Hierarchically formed as material accretes onto them over time, they provide invaluable information towards learning about the structure of matter in the universe. These clusters are 80-90 percent dark matter, with only 15-18 percent being gas in the intra-cluster medium (ICM) and 1-3 percent being the galaxies themselves. One way to study the ICM is through observations of the Sunyaev-Zel'dovich (SZ) effect, which is an inverse compton scattering effect found in the ICM, meaning that hot electrons collide with photons, scattering them to higher frequencies. This indicates that there is less cosmic microwave background (CMB) observable in the area. There are two components of the SZ, thermal and kinetic. For the sake of this research, only the thermal (tSZ) portion will be discussed. The tSZ is proportional to the electron pressure and is thought about in terms of compton y where $y = (\sigma_T/m_e c^2) \int P_e dl$, σ_T is the Thomson cross-section, m_e is the electron mass, P_e is the electron pressure, and c is the speed of light.

The ability to study the structure of galaxy clusters is largely constrained by the mass and redshift, z of the cluster. Finding the mass is crucial for this, just like with other astronomical research because it can allow us to find the distribution and density of gas at different radii from the cluster center, allowing us to learn about the cluster structure. SZ observations allow for the calculation of cluster mass, as well as the analysis of several astrophysical processes in clusters such as shocks, mergers, and sloshing. There are three notable methods to obtain the mass of a cluster from SZ data, the first of which relates P_e to the total pressure while assuming hydrostatic equilibrium. This method is constrained by requiring X-Ray data to be fully functional. The second method requires assuming the virial

Name	RA (h:m:s)	Dec(d:m:s)	T_x (keV)	z	M_{500} ($M_\odot$)
Zw3146	10:23:39.3336	+4:11:14.1248s	7.0	0.291	8e14
MACS J0717+3745-A	07:17:25.0	+37:45:54.6	9.06	2.0e14	0.5458
MACS J0717+3745-B	07:17:31.3	+37:45:30.3	9.06	5.0e14	0.5458
MACS J0717+3745-C	07:17:35.8	+37:45:01.0	9.06	5.0e14	0.5458
MACS J0717+3745-D	07:17:33.0	+37:45:15.0	9.06	2.0e14	0.5458
RXJ 1053+5735-E	10:53:44.7682	+57:35:19.25	7.0	2.0e14	1.14
RXJ 1053+5735-W	10:53:39.445	+57:35:20.59	7.0	2.0e14	1.14
MACS J1149.5+2223	11:49:35.4	+22:25:04	8.5	0.544	19e14

Table 1. The basic properties of each cluster studied in this paper are listed where RA is right ascension, Dec is declination, T_x is ——-, z is redshift and M_{500} is the mass that falls within the radius where the average density of the intra cluster gas is 500 times the critical density of the universe

theorem and a total matter distribution (Navarro, Franklin, and White (NFW), implemented in (Mroczkowski et al. 2012)). The third method, the one used in the models discussed in this paper, as well as in (Arnaud, M. et al. 2010) relies on the scaling relation between the cluster mass and the integrated compton parameter, Y. This paper does not seek to analyze these factors, but rather put in place a better understanding of the noise in our observations so that others can more accurately explore them.

This paper is organized as follows. Section 2 describes the MUSTANG-2 instrument, our observations, and the chosen clusters. Section 3 describes the modeling techniques we used to extract pressure profiles, including our new technique where we implement a covariance matrix of the noise in order to more accurately quantify our noise. Our results are introduced in section 4, including pressure profiles and residuals for the different modeling techniques. Our conclusions are hosted in section 5.

2. INSTRUMENT AND STUDIED CLUSTERS

The observations for this project were done by the MUSTANG2 bolometer on the 100 meter Robert C. Byrd Green Bank Telescope (GBT). MUSTANG2 observes between 75 and 105 GHz primarily because this region is at a minimum of types of emission such as synchrotron and free-free that could obscure SZ observations. Additionally, MUSTANG2 has a resolution of about 10" and a field of view of 4.2'. More information on MUSTANG2 and the data reduction practices associated with it can be found in (Dicker et al. 2020).

The four clusters used in this project are MACS J0717+3745 (MACS J0717), Zw3146, RXJ1053+5735 (RXJ 1053), and MACS J1149.5+2223 (MACS 1149). MACS J0717 has a redshift of 0.5453 and is the most massive galaxy with $z > 0.5$. Furthermore, the cluster presents unique merging behavior with four subclusters, making it quite an interesting system (Jauzac et al. 2018). MACS 1149 is a strong lenser and is frequently studied in addition to being one of the six targets for the *Hubble Frontier Fields* program (Zheng et al. 2017). RXJ 1053 is interesting because it contains a unique double-lobed X-ray morphology (Hashimoto 2005). Zw3146 is one of the most extreme cool-core clusters and is often studied for its brightest cluster galaxy (BCG) (Vantyghem et al. 2021). The information gathered about each of the clusters can be found below in table 1.

3. MODELS

To fit pressure profiles, we use a non-parametric model as in Romero et al. (2018). The model assumes spherical symmetry for the clusters as well as a power law interpolation between radial bins for the pressure profile. The constraints that the bins are chosen include being separated by at least the FWHM of MUSTANG2, with the outermost bin being beyond the FOV. The interpolation between bins is defined as:

$$\alpha = -\frac{\log(P_{i+1}) - \log(P_i)}{\log(R_{i+1}) - \log(R_i)}, \tag{1}$$

where i denotes each bin at radius, r, and $P(r) = P_i(r/R_i)^\alpha$. We restrict α for both the innermost and outermost bins to keep the interpolation from implying the system has infinite mass and a definite integral. This overall method can be used similarly to the generic NFW approach, but offers more flexibility. We calculate the electron pressure as a Compton y parameter:

$$y = \frac{\sigma_T}{m_e c^2} \int P_e dl \tag{2}$$

For the model itself, the basis of our approach is the same as in Romero et al. (2018). We implement maximum likelihood fitting and apply priors in accordance with Bayes' Theorem to attain our probability function. This is equivalent to saying that we are trying to minimize the χ^2 function as in (Romero et al. 2015). This is done with just the pixels of our data and model and not with the included priors:

$$\chi^2 = (\vec{d} - \vec{d_{mod}})^T N^{-1} (\vec{d} - \vec{d_{mod}}), \tag{3}$$

where d is the data, d_{mod} is the model, and N^{-1} is the covariance matrix of the noise. We then use emcee, a Python package built to run Markov Chain Monte Carlo (MCMC) fitting. Throughout that process, we are also keeping track of an integrated Compton y parameter, Y:

$$Y = \int 4\pi y r^2 dr, \tag{4}$$

where $d\Omega$ represents a differential solid angle. This can be done both spherically and cylindrically, but for our purposes, we integrate spherically. This sets the basis of the model used in this paper. Next, the changes will be introduced.

With MIDAS maps created with MUSTANG2 data, previously noise was assumed to be pixel independent, as in the noise in a pixel value has no correlation with the noise in other pixels. This assumption works on small scales, but it fails to hold up on larger scales that analyze the structure of the entire galaxy cluster. To model our noise as dependent, we will take a look at the covariance matrix of our noise from equation 3. When the noise is independent, the covariance matrix only exists along the diagonal, but this changes when we model our noise as dependent. Our proof follows as in Sievers (2020)[1]. We begin with taking the Fourier transform of our noise map, taking us into a frequency domain. From here, we assume that our data is position independent, or the pixel value does not depend on spatial coordinates. This is equivalent to saying that the time ordered data from our observation is time independent. We can then look at the product of the covariance of two different modes of the Fourier transform. This results in:

$$\langle F(k)F(k') \rangle = \left\langle \sum \sum \exp(-2\pi i k x/N) \exp(2\pi i k' x'/N) f(x) f'(x) \right\rangle. \tag{5}$$

We can then set $x' = x + \delta_x$ and $k' = k + \delta_k$, while using the definition of the correlation function $f(x)f(x+\delta_x) = g(\delta_x)$ as well as the Wiener-Khinchin theorem, $\sum_x g(\delta_x) = N g(\delta_x)$ to arrive at:

$$\langle |F(k)|^2 \rangle = \left\langle N \sum_{\delta_x} \exp(2\pi i k \delta_x/N) g(\delta_x) \right\rangle. \tag{6}$$

This states that the quantity on the right, the covariance matrix of the noise, is equal to the power spectrum, which is the squared absolute value of the Fourier transform of the noise. We implement that into our model by taking the fourier transform of the difference between our model and data and multiplying it by the covariance matrix of the noise, essentially just taking the Fourier transform of equation 3.

4. RESULTS

4.1. *Zw3146*

We model Zw3146 as a single spherical cluster with 6 foreground point sources modeled as circular gaussians. Figure 1 shows the comparison of the pressure profiles between the independent noise model and the covariance model. While the models deviate from eachother, they remain statistically in agreement, as determined by their error bars. There seems to be moderate agreement between ACCEPT data (Cavagnolo et al. 2009) and both models, although there no analysis has been done determining the exact degree of said agreement.

[1] Lecture notes found at https://github.com/sievers/phys512-2020/blob/master/notes/stationary_noise.pdf

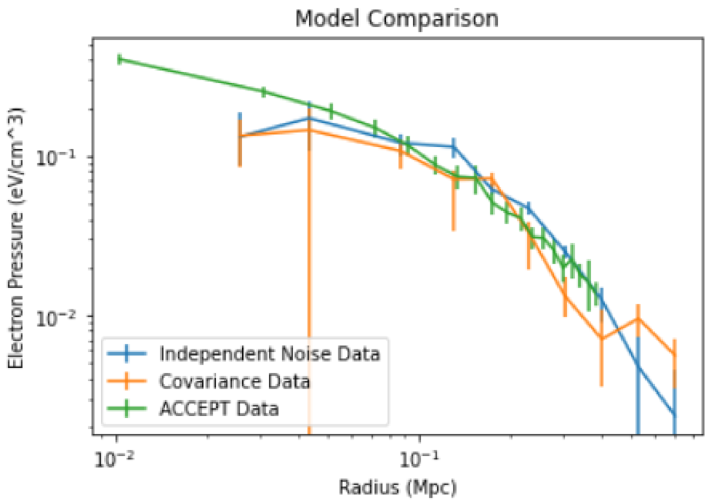

Figure 1. Pressure profile comparison between the independent noise model (blue) and covariance model (orange). The y-axis shows electron pressure while the x-axis shows radius from the cluster center.

4.2. *MACS 0717*

We model MACS 0717 as four separate subclusters with three foreground point sources modeled as circular gaussians. One of the point sources seen to the lower left of the clusters, is more accurately characterized as elliptical, resulting in an inaccuracy of our model. Figure 2 shows the comparison of the pressure profiles between the independent noise model and the covariance model. Just like with Zw3146, the models are statistically in agreement as determined by their error bars. For subclusters A, C, and D, there is almost no agreement between ACCEPT data and the two models, but for subcluster B, there is slight agreement between ACCEPT data and the covariance model, although this has not been statistically measured.

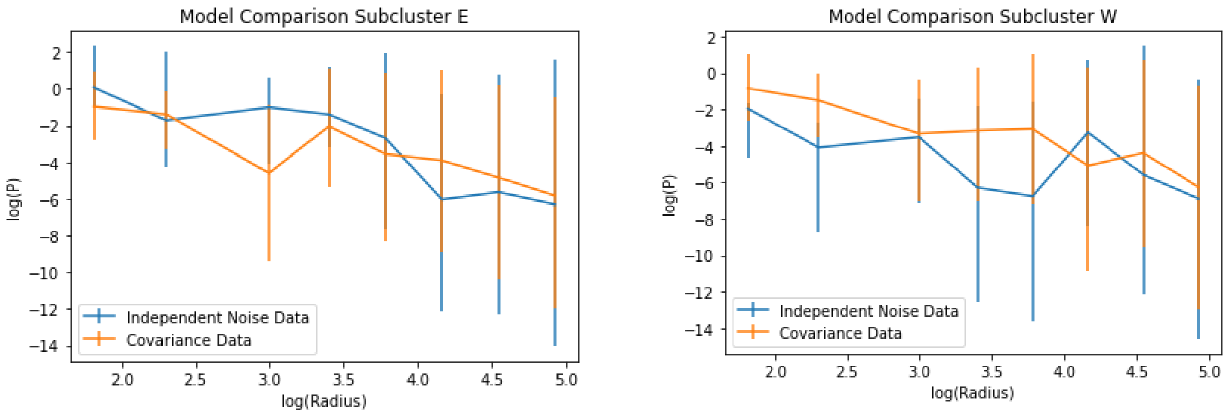

Figure 3. RXJ 1053 results showing subcluster E (left) and subcluster W (right).

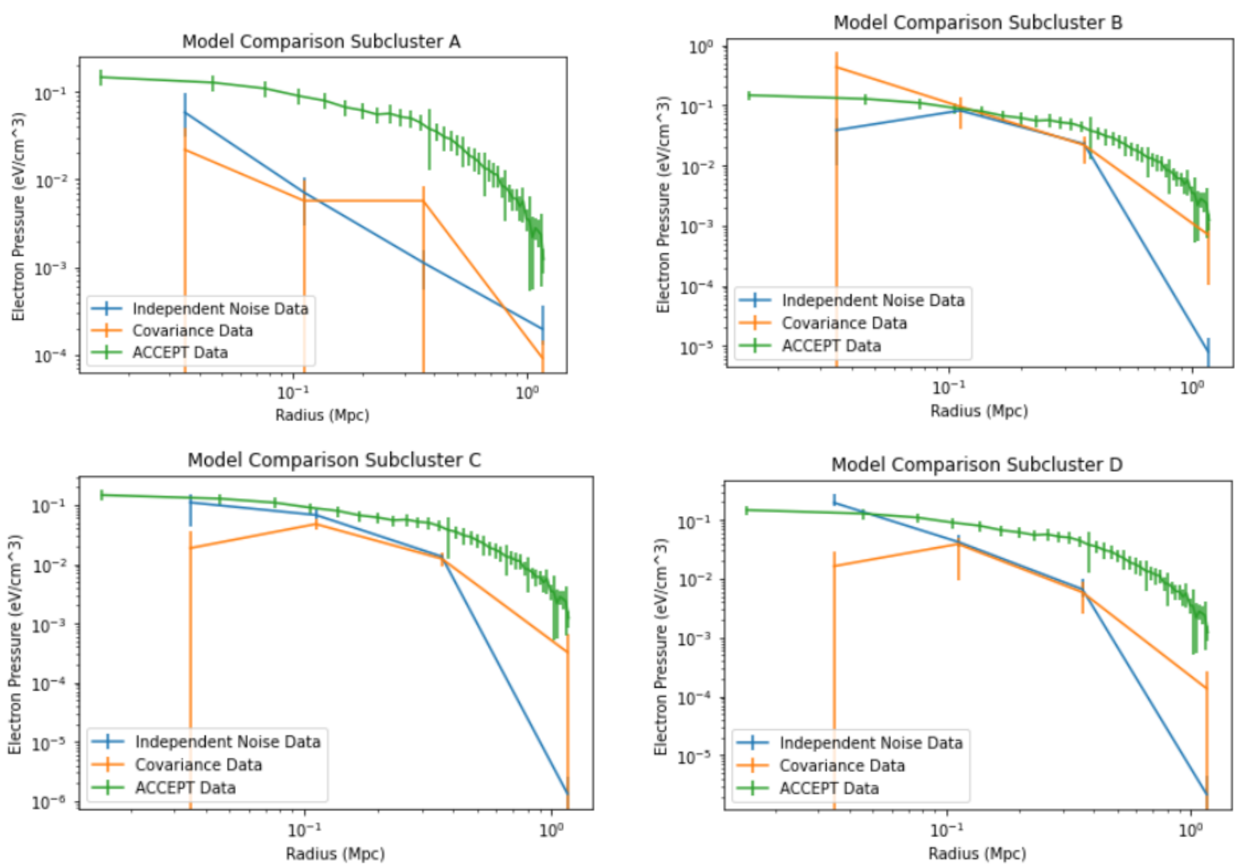

Figure 2. MACS 0717 Results showing subcluster A (upper left), subcluster B (upper right), subcluster C (lower left), and subcluster D (lower right).

4.3. *RXJ 1053*

We model RXJ 1053 as two separate subclusters with an absence of foreground point sources. Figure 3 shows the comparison between the independent noise model and the covariance model. Just like with the previous clusters, both subclusters of RXJ 1053 show statistical agreement, however, the agreement appears to be less clear than in the previous clusters.

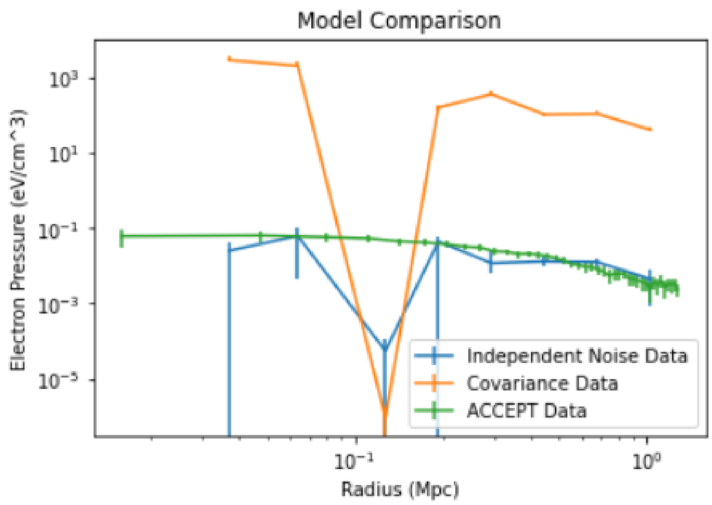

Figure 4. MACS 1149

4.4. *MACS 1149*

We model MACS 1149 as a singular spherical cluster with an individual point source in the foreground. Figure 4 shows the comparison between the independent noise model and the covariance model. Unlike the previous clusters, the two models are in statistical disagreement for all but one of the radial bins. There seems to be a fair amount of agreement between ACCEPT data and the independent noise model, however, this has only been determined by inspection.

5. DISCUSSION

To reiterate the importance of this project, the covariance technique discussed throughout this paper has mostly been used with survey instruments where the assumption that the map data is position independent is more clear. For MUSTANG-2, whether or not this assumption holds is less evident considering our non-uniform weight maps and daisy-pattern observing. However, the motivation for this method comes from a lack of clarity as to whether the noise in MUSTANG-2 MIDAS maps is position independent. While that works on smaller scales, on larger scales there seems to be some relationship between pixel noise. The goal of this project is to implement a model that seeks to better explain this relationship.

We have implemented a technique into our procedure that fits electron pressure profiles of galaxy clusters that models the pixel noise as correlated instead of independent. We performed consistency checks with previously used techniques for MUSTANG-2 MIDAS maps and additionally compared our results with pressure profiles derived from external datasets. We have applied this technique with four clusters and achieved results in agreement with the method in (Romero et al. 2020) with three of the four clusters. Furthermore, we have compared our results for Zw3146, MACS 0717, and MACS 1149 with those from the ACCEPT Catalog and found differing levels of agreement between the independent noise model and the covariance model with the ACCEPT data. While the general shape and scale of the comparisons is reassuring, more research needs to be done to determine the specific levels of agreement and disagreement.

Additionally, our model proved to be succesful in removing point sources, barring an elliptical source in MACS 0717, which introduces a way to improve our point source modeling. We have also modeled the clusters MACS 0717 and RXJ 1053 as being comprised of multiple subclusters while maintaining agreements between the covariance and independent noise models. However, at this point we are lacking an external dataset to compare our results with that could provide insight into which of the two methods discussed in this paper would be preffered so it is not clear which method should be used for future work.

Future analysis of this method could look into why the fitting for MACS 1149 was unsuccessful. Additionally, there is another method of calculating a covariance matrix, as in (Adam et al. 2016) that follows a similar approach that could be compared with the method used in this paper. Furthermore, the method used in this paper could be tested with clusters that have more evident shock features to analyze violently merging clusters. At this stage in the project, we cannot conclude that one noise model performs better over another, thus future work would require finding some means to distinguish between the performance of the two techniques. For that reason, the next step in this project is to be able to determine which of the independent noise and covariance models is preferable. To do this, we need to analyze one or more clusters that have outstanding data on pressure profiles from other instruments. One such cluster to discuss is RXJ 1347.5-1145, which presents a shock region.

APPENDIX

A. CLUSTER MAPS

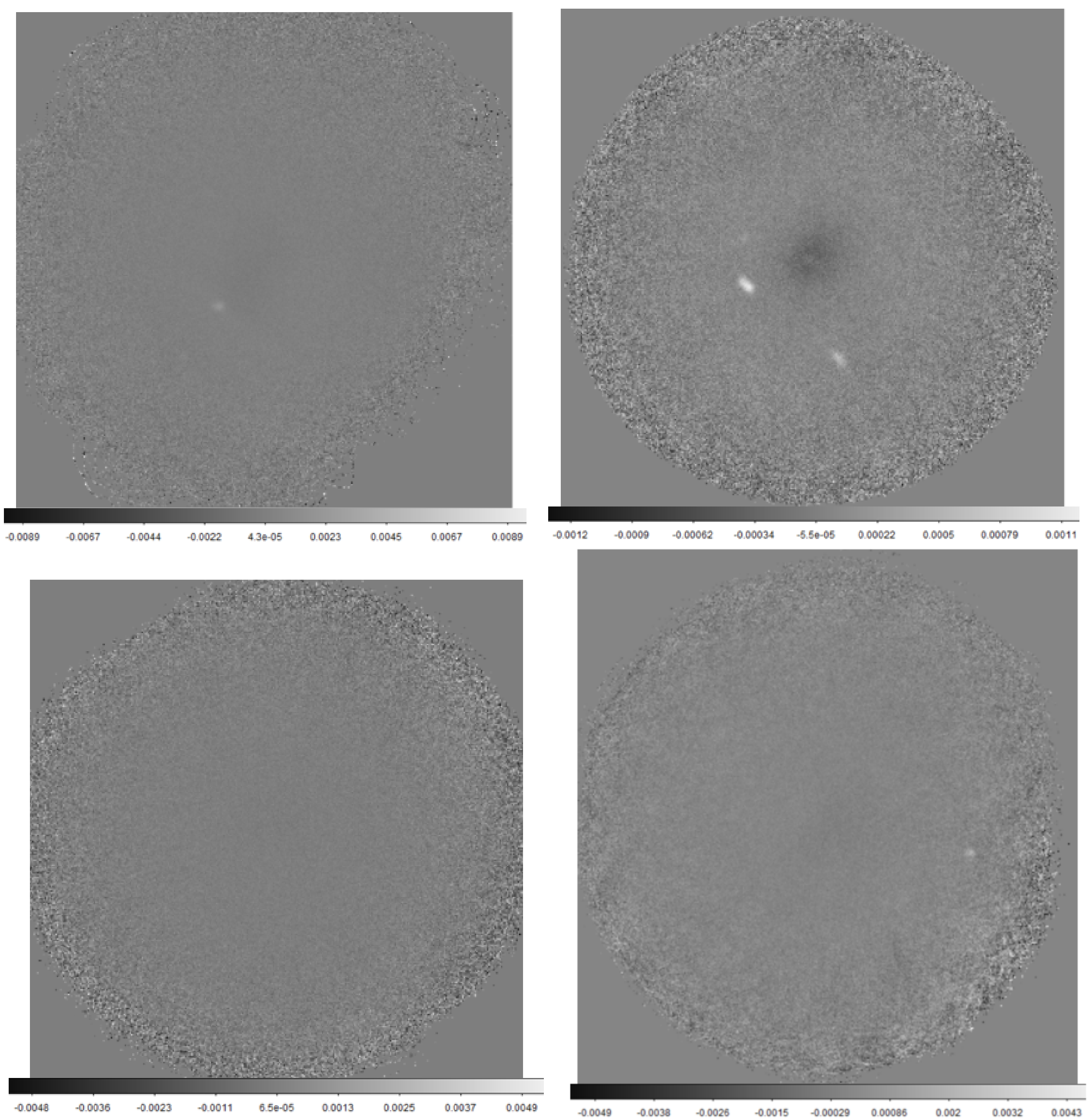

Figure 5. Surface brightness profile of MACS 0717 in Kelvin showing MACS 0717 (upper left), Zw3146 (upper right), RXJ 1053 (lower left), and MACS 1149 (lower right).

B. COVARIANCE MODEL RESIDUAL MAPS

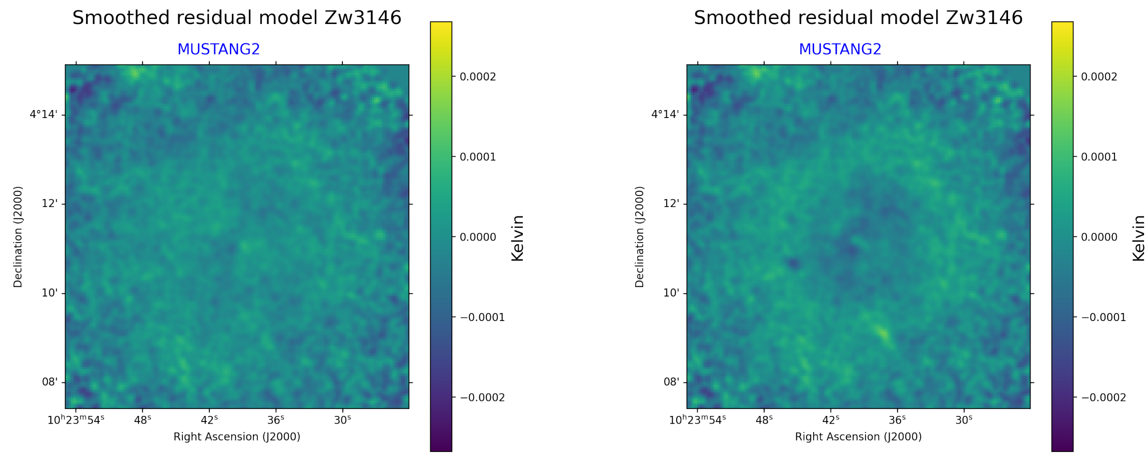

Figure 6. Residual of Zw3146 showing the independent noise model (left) and the covariance model (right).

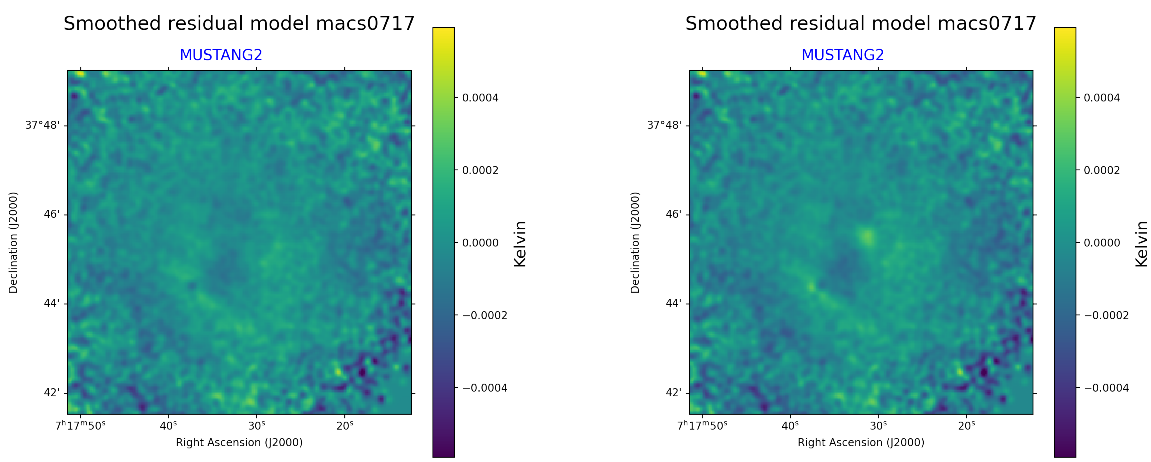

Figure 7. Residual of MACS 0717 showing the independent noise model (left) and the covariance model (right).

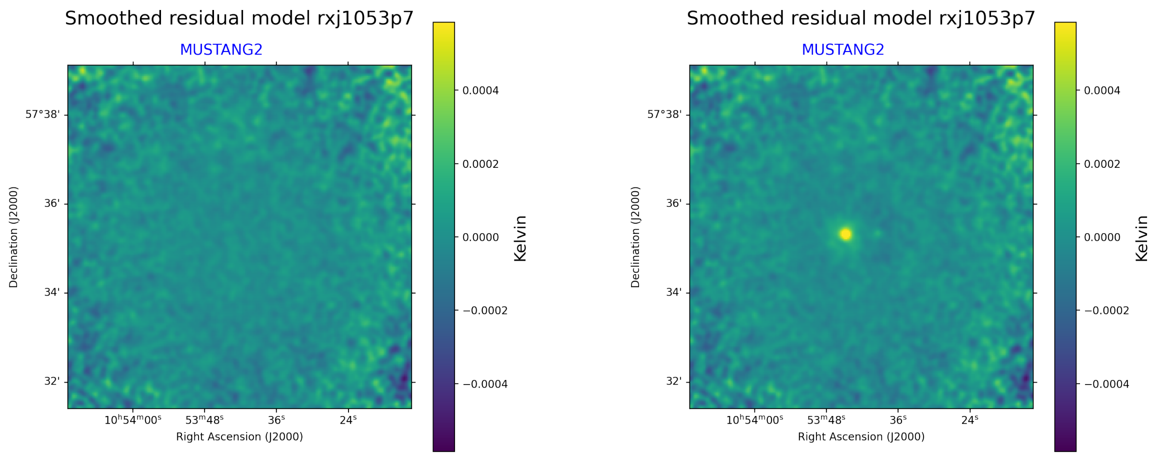

Figure 8. Residual of RXJ 1053 showing the independent noise model (left) and the covariance model (right).

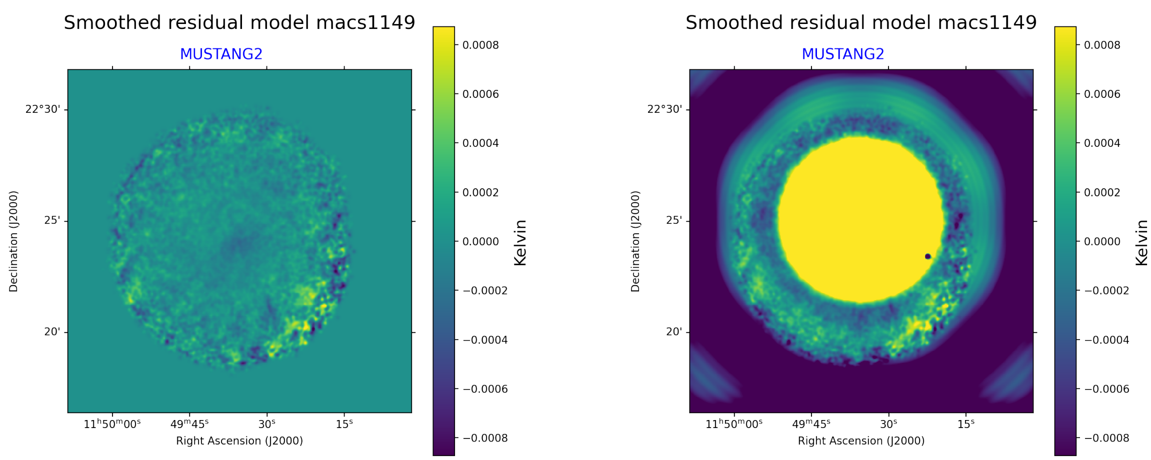

Figure 9. Residual of MACS 1149 showing the independent noise model (left) and the covariance model (right).

REFERENCES

Adam, R., Comis, B., Bartalucci, I., et al. 2016, Astronomy Astrophysics, 586, A122, doi: 10.1051/0004-6361/201527616

Arnaud, M., Pratt, G. W., Piffaretti, R., et al. 2010, A&A, 517, A92, doi: 10.1051/0004-6361/200913416

Cavagnolo, K. W., Donahue, M., Voit, G. M., & Sun, M. 2009, The Astrophysical Journal Supplement Series, 182, 12–32, doi: 10.1088/0067-0049/182/1/12

Dicker, S. R., Romero, C. E., Mascolo, L. D., et al. 2020, The Astrophysical Journal, 902, 144, doi: 10.3847/1538-4357/abb673

Jauzac, M., Eckert, D., Schaller, M., et al. 2018, Monthly Notices of the Royal Astronomical Society, 481, 2901–2917, doi: 10.1093/mnras/sty2366

Mroczkowski, T., Dicker, S., Sayers, J., et al. 2012, The Astrophysical Journal, 761, 47, doi: 10.1088/0004-637x/761/1/47

Romero, C., McWilliam, M., Macías-Pérez, J.-F., et al. 2018, Astronomy Astrophysics, 612, A39, doi: 10.1051/0004-6361/201731599

Romero, C. E., Mason, B. S., Sayers, J., et al. 2015, The Astrophysical Journal, 807, 121, doi: 10.1088/0004-637x/807/2/121

Romero, C. E., Sievers, J., Ghirardini, V., et al. 2020, ApJ, 891, 90, doi: 10.3847/1538-4357/ab6d70

Vantyghem, A. N., McNamara, B. R., O'Dea, C. P., et al. 2021, The Astrophysical Journal, 910, 53, doi: 10.3847/1538-4357/abe306

Zheng, W., Zitrin, A., Infante, L., et al. 2017, The Astrophysical Journal, 836, 210, doi: 10.3847/1538-4357/aa5d55